Metallic magnetism from crystals to amorphous structures in Fe, Co, and Ni

Y. Kakehashi and T. Uchida
Department of Physics, Hokkaido Institute of Technology, Maeda 7-15-4-1, Teine-ku, Sapporo 006, Japan

M. Yu*
Max-Planck Institut für Physik Komplexer Systeme, Bayreuther Strasse 40, Haus 16, D-01187, Dresden, Germany
(Received 15 October 1996)

A theory of metallic magnetism that interpolates between crystals and amorphous structure has been developed on the basis of the functional integral technique and the distribution function method to investigate nonunique magnetism in amorphous Fe, Co, and Ni with different degree of structural disorder. Numerical results of various magnetic moments, susceptibilities, and magnetic phase diagram are presented as a function of the fluctuation of interatomic distance $[(\delta R)^2]_s^{1/2}/[R]_s$, the average coordination number z^*, and temperature. (Here $[\ ]_s$ denotes the structural average.) It is demonstrated that there is a phase transition from the ferromagnetism to the spin glass in Fe with increasing structural disorder. The experimental data of amorphous Fe showing the ferromagnetism (the spin glass) are explained by the parameters $z^* \approx 10.5$ ($z^* \approx 11.5$) and $[(\delta R)^2]_s^{1/2}/[R]_s \approx 0.07$. The Curie temperature (T_C) in Co is shown to increase monotonically with increasing the degree of structural disorder, but to have no maximum between the crystals and amorphous structure, while in Ni, T_C decreases with increasing degree of structural disorder. The latter explains various T_C as found by an extrapolation of the experimental data in Ni-rich amorphous alloys. [S0163-1829(97)03538-8]

I. INTRODUCTION

Much effort has been concentrated on the amorphous metallic magnetism towards understanding magnetic properties of amorphous pure metals and their amorphous alloys close to pure metals in the past decade[1–3] and yielded the discoveries of peculiar magnetic properties of amorphous Fe, Co, and Ni as well as much controversy of their experimental data.

In Fe-rich amorphous alloys containing early transition metals, it was found that the Curie temperatures (T_C) rapidly decrease beyond 80 at. % Fe and spin glasses (SG's) appear beyond 90 at. % Fe.[4–10] Since the SG transition temperatures (T_g) hardly depend on the second elements, it was considered that the SG is caused by the structural disorder being intrinsic in the amorphous pure Fe. In order to elucidate the magnetic phase in Fe-rich amorphous alloys, we developed a finite-temperature theory of amorphous metallic magnetism[11–14] on the basis of the functional integral method[15–17] and the distribution function method.[18] The theory explained the SG of amorphous Fe in a reasonable range of parameters by means of a competition between ferro- and antiferromagnetic interactions due to the nonlinear magnetic couplings and the local environment effects on the amplitude of local magnetic moments.[13]

It is well known, on the other hand, that an extrapolation of magnetization in amorphous Fe_cB_{1-c} ($c<0.9$) alloys yields a large magnetic moment $2.2\mu_B$ for amorphous pure Fe, showing rather strong ferromagnetism (F).[19] The experimental data were often referred to in the literature for the ground-state electronic-structure calculations to justify the theoretical results.[20–22] According to more recent experimental investigations, the amorphous Fe in Y/Fe/Y film shows the ferromagnetism with the ground-state magnetization $1.2\mu_B$ though the magnetization shows the strong thickness dependence.[23] Moreover, the amorphous Fe powders containing 2 wt. % H, 3 wt. % C, and 1 wt. % O were also reported to show the ferromagnetism with the magnetization $1.4\mu_B$ at the ground state.[24]

Apart from the effects of the second elements in the amorphous Fe alloys, one of the possible origins that may cause the contradictory experimental results for amorphous Fe mentioned above is the volume change. We therefore investigated the volume dependence of the magnetism in amorphous Fe and found the F-SG-P transition with decreasing volume.[25] (Here P denotes the paramagnetism.) In particular, we found that the equilibrium volume of amorphous Fe is expected to be close to the phase boundary between F and SG and therefore discussed the possibility of the appearance of ferromagnetism in Y/amorphous Fe/Y film due to volume expansion.

The second origin that can yield nonunique experimental results in amorphous Fe is a detailed change in microscopic amorphous structure. The size difference between Fe and the second elements, the difference in chemical bond with the second elements, and the different preparation techniques may cause different amorphous structures and therefore different magnetic properties.

The nonunique magnetism due to different microscopic structures seems also to be seen in amorphous Ni. As shown in Fig. 1 as an example, the Curie temperatures (T_C) in amorphous Ni-Y,[26] Ni-Zr,[27] and Ni-La (Ref. 28) do not agree even beyond 90 at. % Ni and yield different values of extrapolated T_C for amorphous pure Ni. The concentration dependence of the Weiss constants in liquid Fe-Ni alloys[29] suggests that Ni with liquid structure would be nonmagnetic.

The purpose of the present work is to investigate the metallic magnetism of Fe, Co, and Ni from crystals to amorphous structure to explain nonunique experimental data mentioned above by means of the degree of structural disorder.

We organize our paper as follows. We first develop in

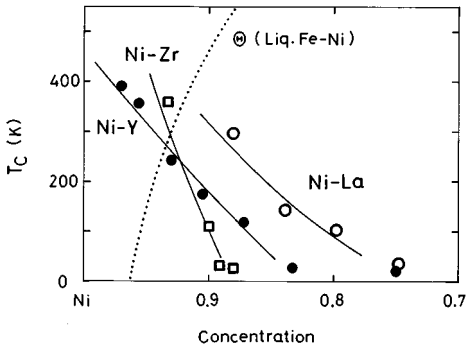

FIG. 1. Curie temperatures in amorphous Ni-Y (●) (Ref. 26), Ni-Zr (□) (Ref. 27), and Ni-La (○) (Ref. 28) alloys. The dotted curve shows the Weiss constant in liquid Fe-Ni alloys (Ref. 29).

Sec. II a theory that describes the finite-temperature magnetism with any degree of structural disorder, interpolating between crystals and amorphous structure. The microscopic atomic structures between the bcc, fcc, and amorphous structures are characterized by an average coordination number z^* and the fluctuations of interatomic distance $\Delta=[(\delta R)^2]_s/[R]_s^2$. Here R is the nearest-neighbor interatomic distance, $[\ ]_s$ denotes the structural average, and $\delta R=R-[R]_s$.

In Sec. III we apply the theory to Fe, Co, and Ni. Various magnetic moments as well as susceptibilities are calculated as a function of z^*, Δ, and temperature T. We will demonstrate in Sec. III A that both ferromagnetism and SG's are possible in amorphous Fe with different z^* and Δ. Moreover, we propose a mechanism of the formation of the reentrant SG's that appear at the boundary between F and SG states.

In Sec. III B we will present the results of calculations for Co and Ni. It is well known experimentally that the Curie temperature of amorphous Co would be enhanced.[30] Estimated T_C is about 1850 K and is 450 K higher than that of fcc Co. Our question in amorphous Co is whether or not the Curie temperature can be enhanced more in the intermediate degree of structural disorder. In the calculation of the magnetism in Ni, we will demonstrate that the different degrees of structural disorder yield different values of T_C. We will realize the ferromagnetism of fcc Ni, a weak ferromagnetism of amorphous Ni, and the nonmagnetic state in Ni with liquid structure. Finally, we summarize our results in Sec. IV.

II. FORMULATION

We briefly review in this section the theory of amorphous metallic magnetism,[11,12,14] and extend it so that one can describe the magnetism in amorphous metals with any degree of structural disorder. In the theory of amorphous metallic magnetism, we start from the degenerate-band Hamiltonian with Coulomb and exchange interactions and apply the functional integral technique.[17] The interacting Hamiltonian is then transformed into a one-electron Hamiltonian with random exchange fields acting on each site. The central local moment (LM) is expressed as a classical average of the field variable ξ on the same site with respect to an energy, which consists of a one-electron free energy with random exchange fields and Gaussian quadratic terms of the random fields [see Eq. (3.15) in Ref. 17].

Introducing effective medium $\mathcal{L}_\sigma$ into the diagonal term of the one-electron Hamiltonian with random exchange potentials, we expand the deviation from the effective medium in the energy functional with respect to the site. By making use of the molecular field approximation for the surrounding field variables, the central LM is given by the number of nearest neighbors (NN's) z, the surrounding LM's $\{\langle m_j\rangle\}$, the squares of transfer integrals $\{y_j=t_{j0}^2\}$, the effective self-energy $\{\mathcal{S}_\sigma\}$ describing the effects of structural disorder outside the NN's, and the effective medium $\{\mathcal{L}_\sigma\}$ describing the thermal spin fluctuations [see Eq. (2.23) in Ref. 12]:

$$\langle m_0\rangle(z,\{\langle m_j\rangle\},\{t_{0j}^2\},\{\mathcal{L}_\sigma^{-1}\},\{\mathcal{S}_\sigma\})=\frac{\int d\xi\,\xi e^{-\beta\Psi(\xi)}}{\int d\xi e^{-\beta\Psi(\xi)}}. \tag{1}$$

Here β denotes the inverse temperature and $\Psi(\xi)$ denotes the energy in the molecular field approximation.

In the disordered system, the surrounding physical quantities z, $\{\langle m_j\rangle\}$, and $\{y_j=t_{j0}^2\}$ show a distribution. We define their distributions as $p(z)$, $g(\langle m_j\rangle)$, and $p_s(y_j)$, respectively. The distribution of the central LM is then obtained from these distributions via Eq. (1). Since it should be identical to the surrounding ones, we obtain an integral equation for the distribution function as [see Eq. (58) in Ref. 14]

$$g(M)=\sum_z p(z)\int \delta(M-\langle m_0\rangle)\prod_{i=1}^{z}[p_s(y_i)dy_i g(m_i)dm_i]. \tag{2}$$

We adopt here the simplest form of $p(z)$:

$$p(z)=([z^*]+1-z^*)\delta_{z,[z^*]}+(z^*-[z^*])\delta_{z,[z^*]+1}, \tag{3}$$

[ ] being Gauss's notation. By making use of the decoupling approximation

$$\int m^{2n+k}g(m)dm\approx[\langle m\rangle^2]_s^n[\langle m\rangle^k]_s \quad (k=0,1), \tag{4}$$

$$\int (y-[y]_s)^{2n+k}p_s(y)dy\approx[(y-[y]_s)^2]_s^n 0^k \quad (k=0,1), \tag{5}$$

we obtain the self-consistent equations for $[\langle m\rangle]_s$ and $[\langle m\rangle^2]_s$ from Eq. (2) [see Eq. (66) in Ref. 14],

$$\begin{bmatrix}[\langle m\rangle]_s\\ [\langle m\rangle^2]_s\end{bmatrix}=\int\begin{bmatrix}M\\ M^2\end{bmatrix}g(M)dM$$
$$=\sum_z p(z)\sum_{n=0}^{z}\Gamma\left(n,z,\frac{1}{2}\right)\sum_{k=0}^{n}\sum_{l=0}^{z-n}\Gamma(k,n,q)$$
$$\times\Gamma(l,z-n,q)\begin{bmatrix}[\langle\xi\rangle(z,n,k,l)]_s\\ [\langle\xi\rangle(z,n,k,l)^2]_s\end{bmatrix}, \tag{6}$$

$$q=\frac{1}{2}\left(1+\frac{[\langle m\rangle]_s}{[\langle m\rangle^2]_s^{1/2}}\right). \tag{7}$$

In the present approximation, the atomic local environment is described by a contraction or a stretch of the NN

atomic distance by $[(\delta R^2)]_s^{1/2}$ on the NN shell since the transfer integrals are connected to the interatomic distance as $t(R) \propto R^{-\kappa}$ ($\kappa = 3.8$ for Fe).[31] Therefore, atomic and spin configurations on the NN shell are expressed by the binomial distribution function $\Gamma(k,n,q)$ defined by $[n!/k!(n-k)!]q^k(1-q)^{n-k}$. $\langle\xi\rangle(z,n,k,l)$ on the right-hand side of Eq. (6) shows the LM's with the local environment specified by z, n (the number of contracted atoms among z NN atoms), k (the number of up spins on the n contracted atoms), and l (the number of up spins on the z-n stretched atoms):

$$\langle\xi\rangle(z,n,k,l) = \frac{\int d\xi \xi e^{-\beta\Psi(\xi,z,n,k,l)}}{\int d\xi e^{-\beta\Psi(\xi,z,n,k,l)}}, \tag{8}$$

$$\begin{aligned}\Psi(\xi,z,n,k,l) = {} & E(\xi,z,n) + n\Phi_+^{(a)}(\xi,z,n) + (z-n) \\ & \times \Phi_-^{(a)}(\xi,z,n) - [(2k-n)\Phi_+^{(e)}(\xi,z,n) \\ & + (2l-z+n)\Phi_-^{(e)}(\xi,z,n)] \frac{[\langle m\rangle^2]_s^{1/2}}{x},\end{aligned} \tag{9}$$

Here x is defined by an amplitude $[\langle\xi^2\rangle_0]_s^{1/2}$ and $\langle\ \rangle_0$ means the thermal average in the single-site approximation.

The single-site energy $E(\xi,z,n)$ on the right-hand side of Eq. (9) is expressed in the D-fold equivalent band model as [see Eq. (3.11) in Ref. 17]

$$\begin{aligned}E(\xi,z,n) = {} & \int d\omega f(\omega) \frac{D}{\pi} \mathrm{Im} \sum_\sigma \ln[L_\sigma(\xi,z,n)^{-1} - \mathcal{L}_\sigma^{-1} \\ & + F_{00\sigma}(z,n)^{-1}] - Nw(\xi,z,n) + \frac{1}{4}\tilde{J}\xi^2,\end{aligned} \tag{10}$$

$$L_\sigma(\xi,z,n)^{-1} = \omega + i\delta - \epsilon_0 + \mu - w(\xi,z,n) + \frac{1}{2}\tilde{J}\xi\sigma + h\sigma. \tag{11}$$

Here $f(\omega)$ denotes the Fermi distribution function, D is the number of degeneracy ($D=5$ for transition metals), N is the d electron number, and $\tilde{J}$ is the effective exchange energy parameter. $\epsilon_0 - \mu$ in Eq. (11) is the atomic level measured from the chemical potential μ, h is the uniform magnetic field, and δ is an infinitesimal positive number.

The charge potential $w(\xi,z,n)$ in Eqs. (10) and (11) is determined from the charge neutrality condition for each local environment (z,n),

$$\begin{aligned}N = {} & \int d\omega f(\omega) \frac{(-D)}{\pi} \mathrm{Im} \sum_\sigma [L_\sigma(\xi,z,n)^{-1} - \mathcal{L}_\sigma^{-1} \\ & + F_{00\sigma}(z,n)^{-1}]^{-1}.\end{aligned} \tag{12}$$

The atomic and exchange pair energies for contracted $(+)$ and stretched $(-)$ pairs in Eq. (9) are given by

$$\begin{bmatrix}\Phi_\pm^{(a)}(\xi,z,n) \\ \Phi_\pm^{(e)}(\xi,z,n)\end{bmatrix} = \frac{1}{2}\sum_{\nu=\pm 1}\begin{bmatrix}1 \\ -\nu\end{bmatrix}\Phi_{\pm 0j}(\xi,\nu x,z,n), \tag{13}$$

$$\begin{aligned}\Phi_{\pm 0j}(\xi,\nu x,z,n) = {} & \int d\omega f(\omega)\frac{D}{\pi} \\ & \times \mathrm{Im}\sum_\sigma \ln[1 - F_{0j\sigma}F_{j0\sigma}^{\pm}\tilde{t}_{0\sigma}(\xi)\tilde{t}_\sigma(\nu x)].\end{aligned} \tag{14}$$

The single-site t-matrices on the central and neighboring sites are expressed as

$$\tilde{t}_{0\sigma}(\xi) = \frac{L_\sigma(\xi,z,n)^{-1} - \mathcal{L}_\sigma^{-1}}{1 + [L_\sigma(\xi,z,n)^{-1} - \mathcal{L}_\sigma^{-1}]F_{00\sigma}(z,n)}, \tag{15}$$

$$\tilde{t}_\sigma(\nu x) = \frac{\overline{L_\sigma}(\nu x)^{-1} - \mathcal{L}_\sigma^{-1}}{1 + [\overline{L_\sigma}(\nu x)^{-1} - \mathcal{L}_\sigma^{-1}]F_\sigma}. \tag{16}$$

Here the locator $\overline{L_\sigma}(\xi)$ in the single-site approximation is defined by Eq. (11) in which the charge potential $w(\xi,z,i)$ has been replaced by the single-site one.

The diagonal and off-diagonal coherent Green's functions at the central site are given in the Bethe approximation as [see Eqs. (2.30) and (2.31) in Ref. 12]

$$F_{00\sigma}(z,n) = \left[\mathcal{L}_\sigma^{-1} - [y]_s K_\sigma\left(z + (2n-z)\frac{[(\delta y)^2]_s^{1/2}}{[y]_s}\right)\right]^{-1}, \tag{17}$$

$$F_{0j\sigma}F_{j0\sigma}^{\pm} = [y]_s\left(1 \pm \frac{[(\delta y)^2]_s^{1/2}}{[y]_s}\right)K_\sigma^2 F_{00\sigma}(z,n)^2, \tag{18}$$

$$K_\sigma = (\mathcal{L}_\sigma^{-1} - \mathcal{S}_\sigma)^{-1}. \tag{19}$$

Here $\delta y = y - [y]_s$.

The averaged coherent Green's function F_σ is calculated from

$$F_\sigma = \sum_{\nu=\pm}\frac{1}{2}\left\{\mathcal{L}_\sigma^{-1} + z^*[y]_s\left(1 + \nu\frac{[(\delta\theta)^2]_s^{1/2}}{[\theta]_s}\right)K_\sigma\right\}^{-1}. \tag{20}$$

Here $\delta\theta = \theta - [\theta]_s$ and $\theta = \Sigma_{j=1}^z y_j$.

The quantities $[(\delta y)^2]_s^{1/2}/[y]_s$ and $[(\delta\theta)^2]_s^{1/2}/[\theta]_s$ in Eqs. (17), (18), and (20) describe the effects of local fluctuations of transfer integrals due to structural disorder on the NN shell. They are expressed by the fluctuations of the interatomic distance $\Delta = [(\delta R)^2]_s/[R]_s^2$ as [see Eqs. (90) and (91) in Ref. 14]

$$\frac{[(\delta y)^2]_s^{1/2}}{[y]_s} = 2\kappa\Delta^{1/2}, \tag{21}$$

$$\frac{[(\delta\theta)^2]_s}{[\theta]_s^2} = \frac{(z^*-[z^*])([z^*]+1-z^*)}{z^*} + \frac{4\kappa^2}{z^*}\Delta, \tag{22}$$

since $t \propto R^{-\kappa}$.

The effective medium $\mathcal{L}_\sigma^{-1}$ is determined from the coherent-potential approximation condition [see Eq. (2.67) in Ref. 12]

$$\sum_{\nu=\pm}\frac{1}{2}\left(1+\nu\frac{[\langle\xi\rangle]_s}{[\langle\xi\rangle^2]_s^{1/2}}\right)\{\overline{L_\sigma^{-1}}(\nu[\langle\xi\rangle^2]_s^{1/2})-\mathcal{L}_\sigma^{-1}+F_\sigma^{-1}\}^{-1}=F_\sigma. \tag{23}$$

Here $[\langle\xi\rangle]_s$ is nothing but $[\langle m\rangle]_s$ and $[\langle\xi^2\rangle]_s$ is given by the upper part of Eq. (6) in which $\langle\xi\rangle(z,n,k,l)$ have been replaced by $\langle\xi^2\rangle(z,n,k,l)$.

Equations (6)–(23) are what we obtained in our previous works[12,14] and show that we can obtain $[\langle m\rangle]_s$ and $[\langle m\rangle^2]_s$ self-consistently once we know the coordination number z^*, the degree of structural disorder Δ, the average band width $z^*[y]_s$, and the effective self-energy $\{\mathcal{S}_\sigma\}$. The latter two quantities are obtained from the average densities of states (DOS) $[\rho(\epsilon)]_s$ for the noninteracting system

$$F_\sigma=\int\frac{[\rho(\epsilon)]_s d\epsilon}{\mathcal{L}_\sigma^{-1}-\epsilon}, \tag{24}$$

$$z^*[y]_s=\int\epsilon[\rho(\epsilon)]_s d\epsilon. \tag{25}$$

We adopted in our previous works[12,13] the DOS $[\rho_a(\epsilon)]$ for amorphous transition metals calculated from an amorphous structure with $z^*=z_a^*$ and $\Delta^{1/2}=\Delta_a^{1/2}$ and obtained the self-energy $\mathcal{S}_{a\sigma}$ and $K_{a\sigma}$, solving Eq. (20) as

$$z_a^* y_a K_{a\sigma}=\frac{2F_{a\sigma}\mathcal{L}_\sigma^{-1}-1\pm\left(1+4\dfrac{[(\delta\theta_a)^2]_s}{[\theta_a]_s^2}F_{a\sigma}\mathcal{L}_\sigma^{-1}(F_{a\sigma}\mathcal{L}_\sigma^{-1}-1)\right)^{1/2}}{2\left(1-\dfrac{[(\delta\theta_a)^2]_s}{[\theta_a]_s^2}\right)F_{a\sigma}}. \tag{26}$$

Here the suffix a is used to specify the quantities for the amorphous structure and the sign should be chosen to be $\mathrm{Im}\,K_{a\sigma}<0$.

The bandwidth parameter $z_a^* y_a$ for amorphous structure is obtained from Eq. (25):

$$z_a^* y_a=\int\epsilon\rho_a(\epsilon)d\epsilon. \tag{27}$$

More important is that the theory also describes the magnetism in crystals. Equations (26) and (27) are then replaced by

$$z_c^* y_c K_{c\sigma}=\mathcal{L}_\sigma^{-1}-F_{c\sigma}^{-1}, \tag{28}$$

$$z_c^* y_c=\int\epsilon\rho_c(\epsilon)d\epsilon. \tag{29}$$

Here the suffix c is added to all the quantities for a crystal ($c=b$ for the bcc, $c=f$ for the fcc), ρ_c denotes the DOS for the crystal, and $F_{c\sigma}$ is the coherent Green's function for crystal given by Eq. (24) in which $[\rho(\epsilon)]_s$ has been replaced by $\rho_c(\epsilon)$.

An orthodox way to calculate the magnetic properties in the intermediate regime of the degree of structural disorder is first to prepare a structure using a method of relaxed dense random packing of a hard-sphere model or a molecular-dynamics method,[3] second to calculate the DOS $[\rho(\epsilon)]_s$ for each structure using a tight-binding linear muffin-tin orbital recursion method,[32] third to calculate F_σ and $z^*[y]_s$ from Eqs. (24) and (25), and finally one has to solve the self-consistent equations (6), (20), and (23). This procedure, however, would require an enormous amount of calculations.

In this paper we adopt a simple interpolation method to obtain $z^*[y]_s$ and K_σ. We assume that the structure in the intermediate regime of structural disorder is approximately described by the parameters z^* and Δ. Moreover, we assume that $z^*[y]_s$ and the self-energy $\mathcal{S}_\sigma$ can be linearly interpolated

$$z^*[y]_s=A+B(z^*-z_a^*)+C\Delta, \tag{30}$$

$$\mathcal{S}_\sigma=A_\sigma+B_\sigma(z^*-z_a^*)+C_\sigma\Delta. \tag{31}$$

The coefficients are determined from the values at three points on the (z^*,Δ) plane (see Fig. 2). Using the crystalline bcc $(z_b^*=8,0)$, the fcc $(z_f^*=12,0)$, and an amorphous structure (z_a^*,Δ_a), we obtain

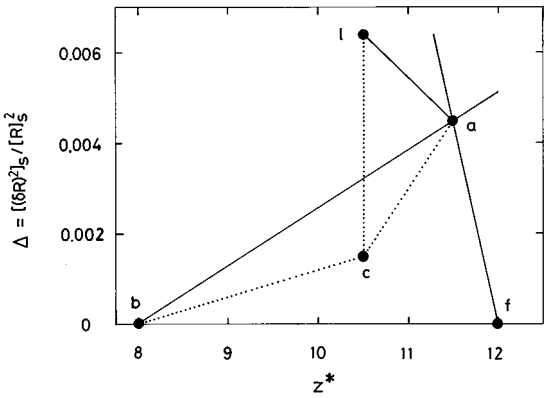

FIG. 2. Amorphous (a), bcc (b), fcc (f), and liquid (l) points and the lines connecting them on the (z^*,Δ) plane. Here z^* is the average coordination number and Δ is the fluctuation of the nearest-neighbor interatomic distance. The point c is the center of gravity for the triangle abf.

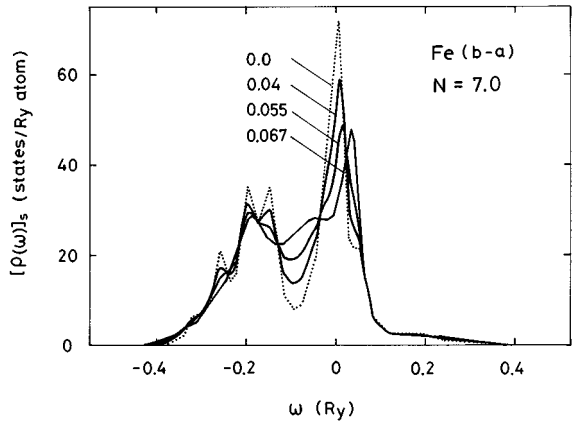

FIG. 3. Noninteracting densities of states (DOS) of Fe for various $\Delta^{1/2}$ (numerals in the figure) along the b-a line. The d electron number is assumed to be $N=7.0$. The dotted curve (the curve for $\Delta^{1/2}=0.067$) shows the input DOS for the bcc (amorphous) structure.

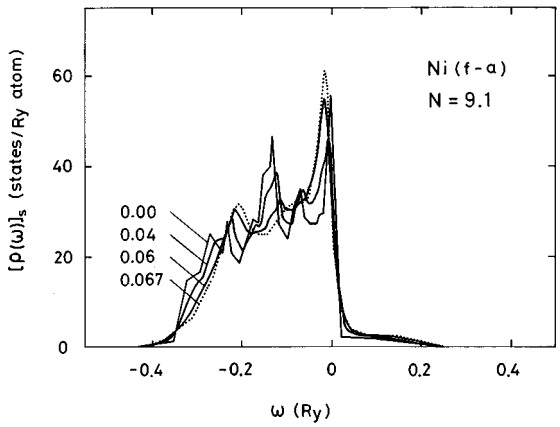

FIG. 4. Noninteracting DOS of Ni ($N=9.1$) for various $\Delta^{1/2}$ (numerals in the figure) along the f-a line. The curve with $\Delta^{1/2}=0.0$ (the dotted curve) shows the input DOS for the fcc (amorphous) structure.

$$z^*[y]_s=\frac{\delta z^*_{ab}}{\delta z^*_{fb}}z^*_f y_f+\frac{\delta z^*_{fa}}{\delta z^*_{fb}}z^*_b y_b+\frac{\delta z^*}{\delta z^*_{fb}}(z^*_f y_f-z^*_b y_b)+\frac{\Delta}{\Delta_a}\left(z^*_a y_a-\frac{\delta z^*_{ab}}{\delta z^*_{fb}}z^*_f y_f-\frac{\delta z^*_{fa}}{\delta z^*_{fb}}z^*_b y_b\right), \tag{32}$$

$$\begin{aligned}(z^*[y]_s K_\sigma)^{-1}=&\frac{\delta z^*_{ab}}{\delta z^*_{fb}}\frac{z^*_f y_f}{z^*[y]_s}(z^*_f y_f K_{f\sigma})^{-1}+\frac{\delta z^*_{fa}}{\delta z^*_{fb}}\frac{z^*_b y_b}{z^*[y]_s}(z^*_b y_b K_{b\sigma})^{-1}\\&+\frac{\delta z^*}{\delta z^*_{fb}}\left[\frac{z^*_f y_f}{z^*[y]_s}(z^*_f y_f K_{f\sigma})^{-1}-\frac{z^*_b y_b}{z^*[y]_s}(z^*_b y_b K_{b\sigma})^{-1}\right]\\&+\frac{\Delta}{\Delta_a}\left[\frac{z^*_a y_a}{z^*[y]_s}(z^*_a y_a K_{a\sigma})^{-1}-\frac{\delta z^*_{ab}}{\delta z^*_{fb}}\frac{z^*_f y_f}{z^*[y]_s}(z^*_f y_f K_{f\sigma})^{-1}-\frac{\delta z^*_{fa}}{\delta z^*_{fb}}\frac{z^*_b y_b}{z^*[y]_s}(z^*_b y_b K_{b\sigma})^{-1}\right].\end{aligned} \tag{33}$$

Here $\delta z^*=z^*-z^*_a$ and $\delta z^*_{ab}=z^*_a-z^*_b$, for example.

We have calculated the change of noninteracting DOS for Fe ($N=7.0$) and Ni ($N=9.1$) as shown in Figs. 3 and 4, using Eqs. (32) and (33), and the average Green's function as[33]

$$[G]_s=\sum_z p(z)\sum_{n=0}^{z}\Gamma\left(n,z,\frac{1}{2}\right)G(z,n), \tag{34}$$

$$G(z,n)=\left[\omega+i\delta-\epsilon_0+\mu-w(0,z,n)-\left\{z-(2n-z)\frac{[(\delta y)^2]^{1/2}_s}{[y]_s}\right\}[y]_s K_\sigma\right]^{-1}. \tag{35}$$

We adopted the input DOS for Fe calculated by Moruzzi *et al.*[34] (the fcc structure; see Fig. 3) and Fujiwara[35] (the bcc and amorphous structures; see Fig. 4). For Ni, we assumed the same input DOS, but their bandwidths were scaled by the ratio 0.364/0.441, i.e., the width of fcc Ni divided by that of fcc Fe.[34] Moreover, we adopted $z^*_a=11.5$,[36,37] $z^*_b=8$, $z^*_f=12$, and $\Delta^{1/2}_a=0.067$.[36,37] The structural disorder is introduced along the c-a line on the (z^*,Δ) plane: $z^*=z^*_c+(z^*_a-z^*_c)\Delta/\Delta_a$ ($c=b$ for Fe and $c=f$ for Ni; see Fig. 2).

Calculated DOS's continuously change from one to another by varying Δ from 0 to Δ_a. In particular, the valley of the DOS near -0.01 Ry in Fe is gradually filled up and the main peak near the top of the DOS shifts to the higher-energy region with increasing Δ, while the peak near the center of the DOS in Ni is worn out by introducing the degree of structural disorder.

Solving the self-consistent equations for $[\langle m\rangle]_s$ and $[\langle m\rangle^2]_s$ [Eq. (6)], $w(\xi,z,n)$ [Eq. (12)], and $\mathcal{L}_\sigma$ [Eq. (23)] together with Eqs. (30) and (31), we obtain the magnetic properties of itinerant electron systems from crystals to amorphous structures. Other magnetic properties such as the amplitude of the LM $[\langle\mathbf{m}^2\rangle]$ and a static spin correlation $[\langle m_0\rangle\langle m_1\rangle]_s$ between the neighboring LM's $\langle m_0\rangle$ and $\langle m_1\rangle$ are obtained as (see the Appendix in Ref. 39)

$$[\langle\mathbf{m}^2\rangle]_s=3N-\frac{3}{2D}N^2+\left(1+\frac{1}{2D}\right)\left([\langle\xi^2\rangle]_s-\frac{2}{\beta\tilde{J}}\right), \tag{36}$$

$$[\langle m_0\rangle\langle m_1\rangle]_s=\frac{1}{z^*}\left[\langle m_0\rangle\sum_j^z\langle m_j\rangle\right]_s$$
$$=\frac{1}{z^*}\sum_z p(z)\sum_{n=1}^{z}\Gamma\left(n,z,\frac{1}{2}\right)$$
$$\times\sum_{k=0}^{n}\sum_{l=0}^{z-n}\Gamma(k,n,q)\Gamma(l,z-n,q)\langle\xi\rangle(z,n,k,l)$$
$$\times[2(k+l)-z]. \quad (37)$$

The present theory takes into account the fluctuations due to structural disorder as well as thermal spin fluctuations. In the crystalline limit, the theory reproduces quantitatively the Stoner model obtained in the band calculations at the ground state and also reproduces quantitatively the Curie temperatures obtained with use of full d orbitals within the single-site approximations[38] because of the inclusion of Hund's rule coupling. In the limit of the amorphous structure, it quantitatively reproduces the average local densities of states obtained from the first-principles band-structure calculations[14,39,40] and describes the spin-glass states caused by the structural disorder at finite temperatures. In the intermediate region of structural disorder, the theory interpolates between the two limits with use of two basic parameters: the average coordination number z^* and the degree of structural disorder Δ.

We used the D-fold equivalent band model in the present theory. The model is suitable for the theory based on the Bethe-type approximation and greatly reduces computing time in the numerical calculations. The use of the full d orbitals in the calculations does not introduce any new aspect within the Bethe-type approximation, though it would be significant if the Bethe-type approximation were overcome. The problem of the directional bonding and its fluctuations due to structural disorder associated with the three-body correlations and the angular part of d orbital is left for future work.

III. NUMERICAL RESULTS

A. Iron

As has been mentioned in the Introduction, the magnetism of Fe is expected to be very sensitive to the structural disorder. In this subsection we investigate the magnetic properties of Fe varying (z^*,Δ) along the lines b-a, b-c-a, and c-l in Fig. 2. We adopted $N=7.0$ and $\tilde{J}=0.059\,045$ Ry, which have been used in our previous works.[11,13,14] A set of parameters leads to the ground-state magnetization $2.216\mu_B$ for bcc Fe. Other input parameters were given in the preceding section.

In Fig. 5 we show various magnetic moments and static spin correlations between the NN LM's at 50 K as a function of Δ along the line b-a. Calculated magnetization gradually decreases first with introducing structural disorder. It begins to show the ferromagnetic instability beyond $\Delta^{1/2}\approx 0.05$ and finally disappears at $\Delta^{1/2}=0.0583$. At this point, Fe shows the transition from the ferromagnetism to the SG since the SG order parameter $[\langle m\rangle^2]_s^{1/2}$ remains beyond $\Delta^{1/2}=0.0583$, as seen in Fig. 5.

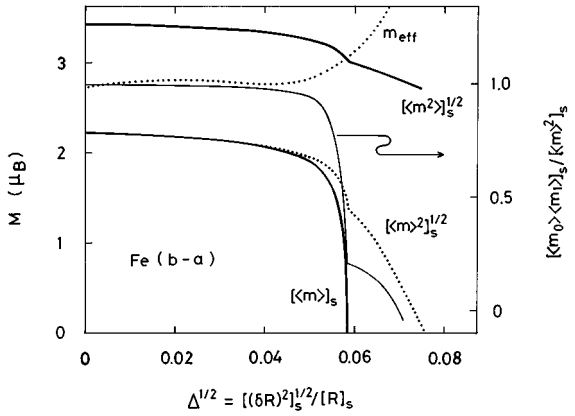

FIG. 5. Various magnetic moments of Fe ($[\langle m\rangle]_s$, the lower solid curve; $[\langle m\rangle^2]_s^{1/2}$, dotted curve; $[\langle m^2\rangle]_s^{1/2}$, the upper solid curve) at 50 K and the effective Bohr magneton number ($m_{\rm eff}$, dotted curve) along the b-a line. The nearest-neighbor (NN) static spin correlation at 50 K ($[\langle m_0\rangle\langle m_1\rangle]_s/[\langle m\rangle^2]_s^{1/2}$) is also presented by the thin solid curve.

These behaviors are explained by the gradual decrease of the noninteracting DOS at the Fermi level caused by the shift of the main peak to the higher-energy region, as shown in Fig. 3. It should be noted, however, that the ferromagnetic instability occurs before the Stoner instability point ($\Delta^{1/2}=0.0635$) where the condition $[\rho(0)]_s\tilde{J}/2=1$ is satisfied. This shows that the disappearance of the ferromagnetism is realized by the reversal of LM's with increasing Δ. In fact, we find such a reversal of LM's in the distribution function $g(M)$, as shown in Fig. 6. The width of the distribution function $g(M)$ first increases around the average value of LM's [see $g(M)$ at $\Delta^{1/2}=0.040$]. A further increase of Δ causes the reversal of LM's [see $g(M)$ at $\Delta^{1/2}=0.055$ and 0.0575] and yields a broad distribution of LM's (from $-2.6\mu_B$ to $2.6\mu_B$) in the SG state at $\Delta^{1/2}=0.060$.

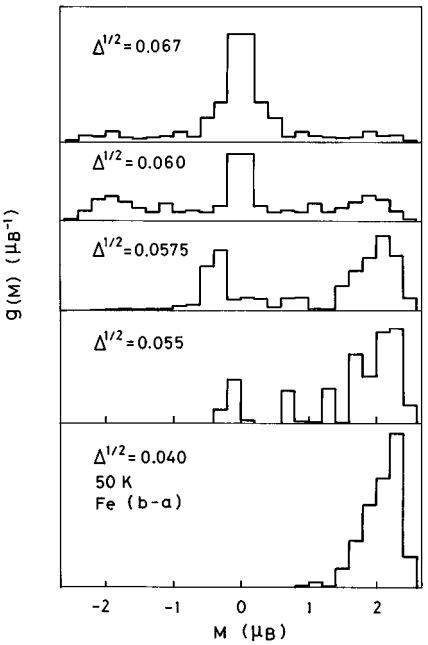

FIG. 6. Calculated distribution functions of Fe local moment (LM) $[g(M)]$ at 50 K for various $\Delta^{1/2}$ along the b-a line.

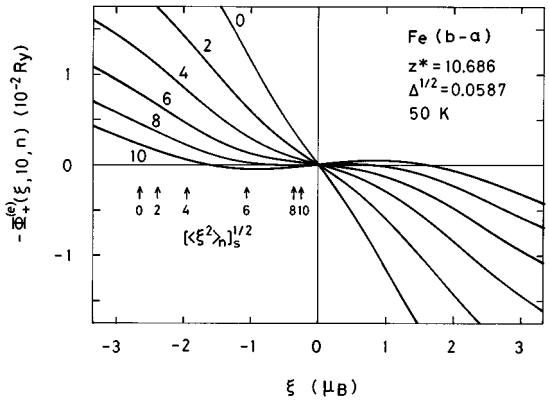

FIG. 7. Exchange pair energies $[-\Phi_{+}^{(e)}(\xi,10,n)]$ of amorphous Fe ($z^*=10.686$ and $\Delta^{1/2}=0.0587$) for various local environments (n is the number of contracted atoms on the NN shell, which are shown by the numerals in the figure). Arrows indicate the amplitude $[\langle\xi^2\rangle_n]_s^{1/2}$ under the given environment n.

The NN magnetic couplings at $\Delta^{1/2}=0.060$ are mainly ferromagnetic, as shown in Fig. 7. [Note that $-\Phi_{+}^{(e)}(\xi,z,n)$ means the magnetic energy gain of the central LM when the neighboring LM with amplitude x points up.] Therefore, the SG state in this region is regarded as the cluster SG with NN ferromagnetic spin correlations. The formation of the SG is caused by the competition between the NN ferromagnetic interactions and the long-range antiferromagnetic ones via effective medium.[11] On the other hand, the NN magnetic couplings for $\Delta^{1/2}=0.07$ possess the strong nonlinearity of the S-type curves as shown in Fig. 8. This means that the central LM's with large amplitude $|\xi|$ ferromagnetically couple to the neighboring LM's, while the LM's with small amplitudes antiferromagnetically couple to the neighboring ones. Since the amplitudes of LM's are strongly influenced by their local environments, the nonlinear magnetic couplings cause the competition between the ferro- and antiferromagnetic NN couplings and therefore the SG around $\Delta^{1/2}=0.07$ due to structural disorder. The two kinds of mechanisms for the formation of SG's mentioned above also explain why calculated NN spin correlations shown in Fig. 5 are ferromagnetic around $\Delta^{1/2}=0.06$, while they almost disappear or even show the antiferromagnetic correlations around $\Delta^{1/2}=0.07$.

Temperature variations of calculated magnetic moments and inverse susceptibilities are presented in Fig. 9 for various

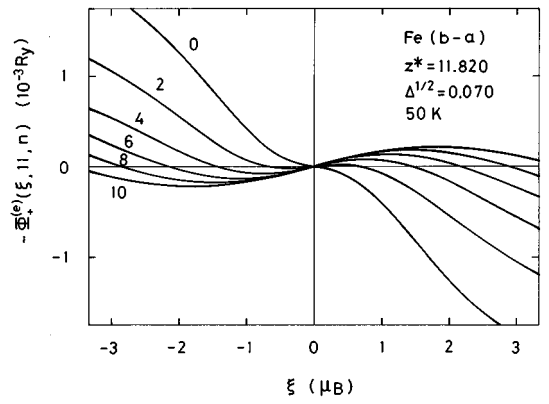

FIG. 8. Same as in Fig. 7, but $z^*=11.820$ and $\Delta^{1/2}=0.070$.

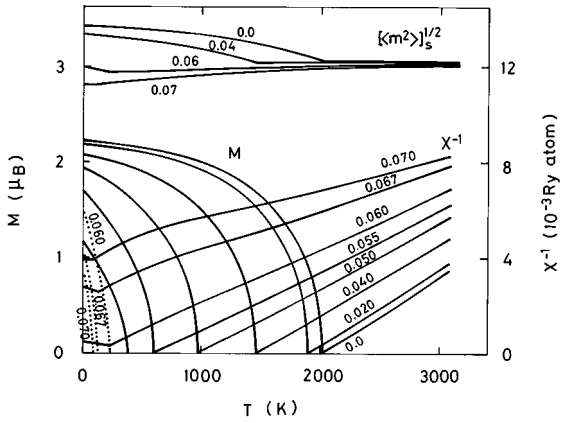

FIG. 9. Magnetizations ($M=[\langle m\rangle]_s$), the spin-glass order parameter ($[\langle m\rangle^2]_s^{1/2}$, dotted curves), inverse susceptibilities (χ^{-1}), and the amplitudes of LM ($[\langle m^2\rangle]_s^{1/2}$) in Fe as functions of temperature T for various $\Delta^{1/2}$, which are shown by the numerals in the figure.

degrees of structural disorder Δ along the b-a line. The magnetization vs temperature (M-T) curve for bcc Fe approximately follows the Brillouin curve. When we increase Δ, the magnetization as well as the Curie temperature decreases and the M-T curve deviates downward from the Brillouin one. The amplitudes of LM's show a rather small temperature variation and keep a constant value of about $3\mu_B$ above the Curie temperature.

Calculated inverse susceptibilities (χ^{-1}) follows the Curie-Weiss law at high temperatures, as seen from Fig. 9. The effective Bohr magneton numbers obtained at high temperatures ($\sim$2000 K) gradually increase as the ferromagnetism is weakened with the introduction of structural disorder (see Fig. 5). The inverse susceptibilities deviate from the Curie-Weiss law for $\Delta^{1/2}=0.067$ and 0.070, and show upward convexity by a linear temperature variation of the amplitude of LM's ($\langle\xi^2\rangle$).[39]

We obtained the magnetic phase diagram from the temperature variations of LM's shown in Fig. 9. The result is presented in Fig. 10. The calculated Curie temperature T_C in the bcc Fe is 2020 K, which is overestimated by a factor of 2 as compared to the experimental value (1040 K) because of

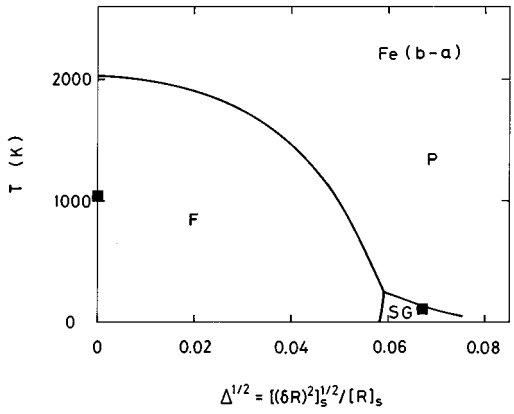

FIG. 10. Magnetic phase diagram of Fe along the b-a line. F, SG, and P indicate the ferromagnetism, the spin glass, and the paramagnetism, respectively. The experimental Curie temperature for bcc Fe and the SG temperature[1,12] are shown by ■.

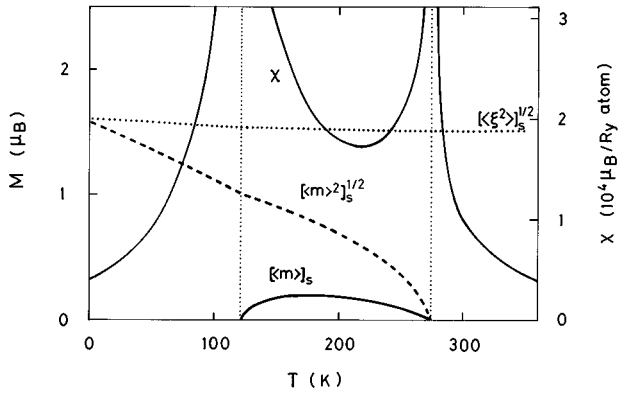

FIG. 11. Magnetization ($M=[\langle m\rangle]_s$), the SG order parameter ($[\langle m\rangle^2]_s^{1/2}$), amplitude ($[\langle\xi^2\rangle]_s^{1/2}$), and susceptibility ($\chi$) of Fe as a function of temperature (T) near the F-SG boundary at $\Delta^{1/2}=0.0587$ on the b-a line.

the molecular field approximation in our theory. It monotonically decreases with increasing Δ along the b-a line. The ferromagnetism completely disappears at ($z^*=10.72, \Delta^{1/2}=0.059$) and the SG appears beyond it. Calculated SG transition temperatures T_g vary from 240 K ($\Delta^{1/2}=0.059$) to 90 K ($\Delta^{1/2}=0.070$). The SG found in Fe-rich amorphous alloys with more than 90 at. % Fe (Refs. 1, and 4–7) can be explained by the present theory if $0.06\lesssim\Delta^{1/2}\lesssim 0.07$. The fluctuation of the interatomic distance $\Delta^{1/2}$ obtained from the recent x-ray experiment is 0.068 (Ref. 36) for $Fe_{90}La_{10}$ amorphous alloys showing the SG. The SG temperatures in Fe-rich alloys are about 110 K beyond 90 at. % Fe, irrespective of the second element.[1] These results are consistent with our phase diagram.

As seen from the calculated phase diagram (Fig. 10), there is a narrow region $0.058\lesssim\Delta^{1/2}\lesssim 0.059$ showing the reentrant spin glass (RSG). A typical temperature variation of the LM and susceptibility is shown in Fig. 11 for $\Delta^{1/2}=0.0587$. The magnetization appears at $T_g=122$ K and shows the maximum at 180 K. The susceptibilities in the RSG are huge, as shown in Fig. 11 [note that $\chi=1.2$ ($10^2\mu_B$/Ry atom) for bcc Fe at room temperature), and show the divergence at both T_g and T_C.

In our previous papers we attributed the RSG behaviors to the detailed balance between short-range ferro- and antiferromagnetic interactions, which is dominated by the amplitude fluctuations. The amplitude ($[\langle\xi^2\rangle]_s^{1/2}$) in the present case, however, hardly changes with increasing temperatures, as shown in Fig. 11. To examine the mechanism for the formation of the RSG, we present the distributions of LM's near the SG-F boundary and the susceptibilities in various local environments in Figs. 12 and 13, respectively.

As seen from Fig. 7, the LM's with more than seven contracted atoms on the NN shell have a small magnitude of LM's and show weak antiferromagnetic couplings with neighboring LM's, while the LM's with fewer than six contracted atoms have a large amplitude of LM's and show the strong ferromagnetic couplings. The former LM's mainly contribute to the distribution of the region $|M|\lesssim 1\mu_B$ and the latter to that of $|M|\gtrsim 1\mu_B$ in the distribution function $g(M)$ at 50 K shown in Fig. 12. When the temperature is raised, the LM's having weak antiferromagnetic couplings

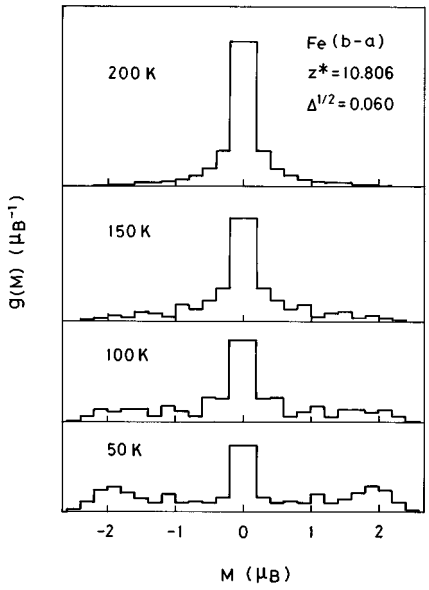

FIG. 12. Temperature variation of the distribution function $[g(M)]$ of Fe near the F-SG phase boundary along the b-a line.

first ''melt'' and the paramagnetic component at $M=0$ develops. There is a temperature region where the most of the LM's having weak antiferromagnetic couplings melt, but the LM's having strong ferromagnetic couplings still remain [e.g., $g(M)$ at 150 K]. The ferromagnetic couplings are relatively enhanced there; therefore, the RSG behavior can be realized. The calculated local susceptibilities for the LM's $[\langle m\rangle_n]_s$ with $n\lesssim 3$ near T_g are enhanced several times, although they are enhanced only a few times for $n\gtrsim 7$, as shown in Fig. 13. This behavior supports the mechanism for the RSG mentioned above.

We have also performed the same calculations along the b-c-a line. The results are presented in Figs. 14 and 15. With increasing Δ, both the magnetization and the Curie

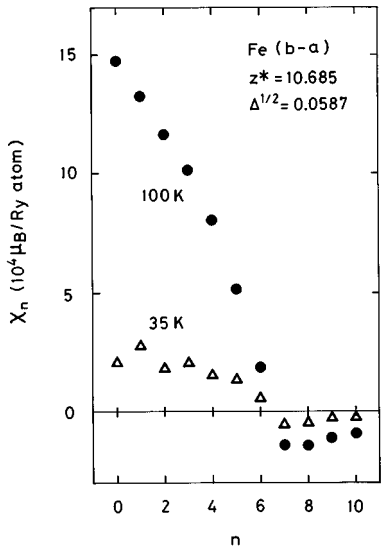

FIG. 13. Local susceptibilities (χ_n) of Fe in various environments specified by n, the number of contracted atoms on the NN shell at 35 K (△) and 100 K (●) in the SG state near the F-SG phase boundary along the b-a line.

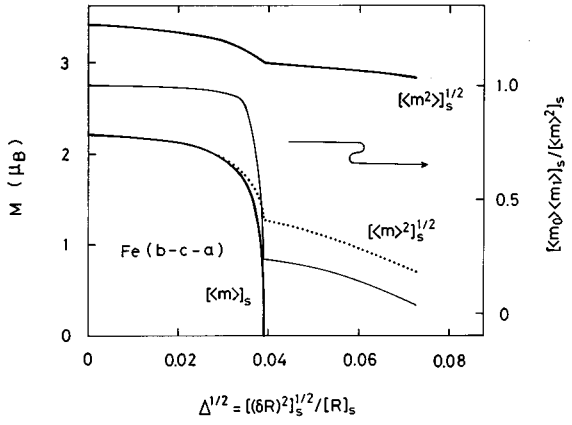

FIG. 14. Same as in Fig. 5, but the results along the *b*-*c*-*a* line.

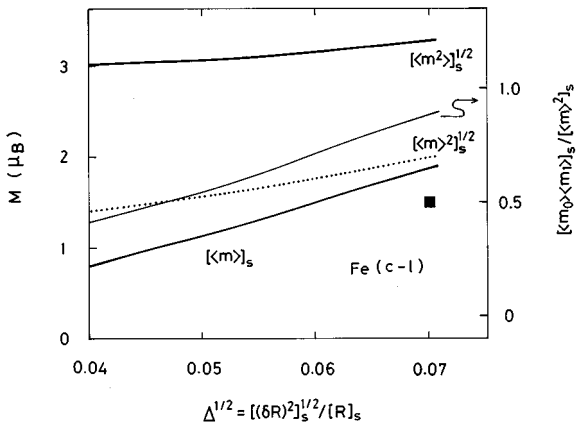

FIG. 16. Same as in Fig. 5, but the results along the *c*-*l* line. The experimental point for amorphous Fe containing 2 wt. % H, 3 wt. % C, and 1 wt. % O (Ref. 24) is shown by ■.

temperature decrease, showing behaviors similar to the results along the *b*-*a* line. The RSG behavior occurs in the range $0.037<\Delta^{1/2}<0.042$ along the *c*-*a* line and the SG appears beyond $\Delta^{1/2}=0.042$ on the line. The critical values $z^*=10.57$, $\Delta^{1/2}=0.042$ for the ferromagnetic instability are smaller than those along the *b*-*a* line, i.e., $z^*=10.72$, $\Delta^{1/2}=0.059$.

The remaining problem in connection to the experimental data is why the amorphous Fe containing H, C, and O impurities and amorphous Fe inferred from Fe-B alloys[19] show ferromagnetism instead of the SG. We examined the radial distribution function for the former[24] and obtained the value $z^*\approx 10.5$, which is smaller than the value $z^*\approx 11.0$ obtained from amorphous $Fe_{90}La_{10}$ alloys,[36] although the $\Delta^{1/2}$ are approximately the same for both systems. We therefore calculated the magnetic moments along the *c*-*l* line in which $z^*\approx 10.5$. Figure 16 shows that the calculated magnetization increases with increasing $\Delta^{1/2}$ and becomes comparable to the experimental value $1.4\mu_B$ around $\Delta^{1/2}=0.07$. Thus the ferromagnetism of amorphous Fe with H, C, and O impurities is explained by a smaller coordination number $z^*\approx 10.5$, which is rather close to the liquid value.

B. Cobalt and nickel

Cobalt and nickel do not have any competing interaction, but their ferromagnetism is expected to be changed by the structural disorder. We present first the results of calculations for Co. We adopted the same input DOS as in Fe since the shapes of the DOS's are known to be common to 3*d* transition metals for the same crystal structure. The bandwidths are scaled commonly by the ratio 0.393/0.441, the ratio of the bandwidth of fcc Fe to that of fcc Co.[34] The *d* electron number is assumed to be $N=8.1$ and the effective exchange energy parameter $\tilde{J}=0.100$ Ry for Co. These values have been used in our previous works[13] and yield the ground-state magnetizations $1.57\mu_B$ for the amorphous structure, $1.51\mu_B$ for the bcc structure, and $1.69\mu_B$ for the fcc structure. The values should be compared with the experimental values $1.72\mu_B$, $1.53\mu_B$, and $1.74\mu_B$, respectively.

The results of calculations for Co are presented in Fig. 17. The magnetization at 150 K hardly changes with increasing the degree of structural disorder along the *f*-*a* line. The width of the LM distribution is also very small because of the strong ferromagnetism with no competition ($([\langle m\rangle^2]_s-[\langle m\rangle]_s^2)^{1/2}\approx 0.05\mu_B$ at 300 K and $\Delta^{1/2}=0.06$ along the *f*-*a* line, for example). The calculated Curie temperatures for fcc and bcc structures are 2480 K and 2680 K

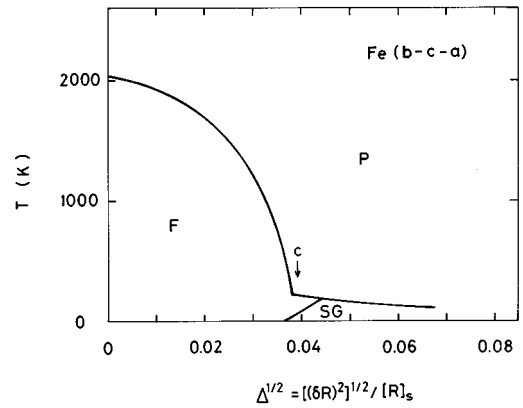

FIG. 15. Same as Fig. 10, but the result along the *b*-*c*-*a* line. The arrow shows the point *c* defined in Fig. 2.

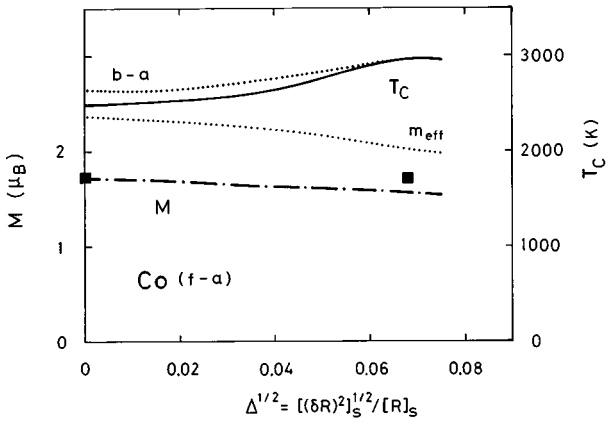

FIG. 17. Magnetization at 150 K (M), Curie temperature (T_C), and the effective Bohr magneton number ($m_{\rm eff}$) of Co as a function of $\Delta^{1/2}$ along the *f*-*a* line. The dotted curve for T_C is the result along the *b*-*a* line. The experimental ground-state magnetization for the fcc and amorphous Co are shown by ■ (Ref. 30).

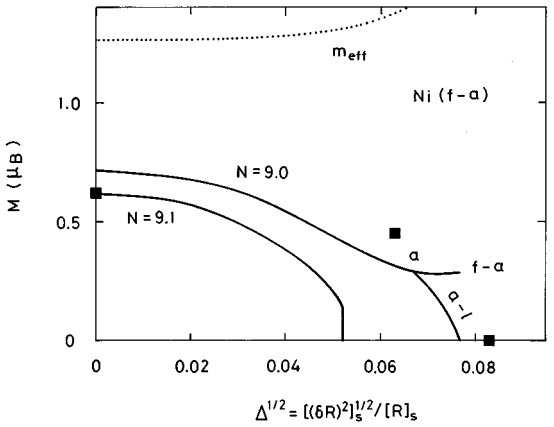

FIG. 18. Calculated magnetizations (M, solid curves) at 50 K and the effective Bohr magneton number (m_{eff}, dotted curve) for Ni ($N=9.0$) along the f-a line. The solid curve with a-l shows the magnetization curve along the a-l line. The result of M for the d electron number $N=9.1$ is also presented. The experimental ground-state magnetization for the fcc and amorphous Ni are shown by ■ (Refs. 26 and 44).

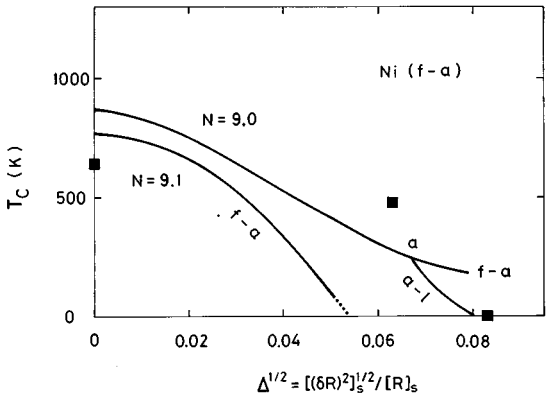

FIG. 19. Calculated Curie temperature along the f-a line for $N=9.0$ and 9.1. The Curie temperature along the a-l line is also presented. The experimental data for fcc, amorphous (Refs. 26 and 41), and liquid (Refs. 29 and 42) structures are shown by ■.

respectively, which are overestimated by a factor of 1.8 as compared to the experimental values [1400 K for fcc Co and 1500 K for bcc Co (Ref. 43)] because of the molecular field approximation. The Curie temperature T_C gradually increases with increasing $\Delta^{1/2}$ and tends to saturate around $\Delta^{1/2}=0.07$. The enhancement of strong ferromagnetism has been explained by the magnetic energy gain associated with the shift of the main peak in the noninteracting DOS to the Fermi level due to structural disorder.[13] The curve for T_C along the b-a line also shows the similar behavior. It turns out that there is no maximum of T_C in the intermediate region of degree of structural disorder. Therefore, it is impossible theoretically to increase T_C by annealing the amorphous structure in Co-rich amorphous alloys. We have also calculated the paramagnetic susceptibilities along the f-a line. They follow the Curie-Weiss law. The calculated effective Bohr magneton number does not show a drastic change with increasing structural disorder, as shown in Fig. 17.

In the case of Ni, we adopted the input DOS for Fe scaling the bandwidth by the ratio 0.364/0.393 for fcc and bcc structures[34] and the ratio 0.262/0.393 for amorphous structures. In the evaluation of the latter ratio, the effects of volume change were taken into account. We adopted the d electron numbers $N=9.0$ and 9.1, since the results are rather sensitive to N, and the effective exchange energy parameters $\tilde{J}=0.060$ Ry. The set of these parameters yields the ground-state magnetizations $0.72\mu_B$ ($N=9.0$) and $0.63\mu_B$ ($N=9.1$) for fcc Ni, which should be compared with the experimental value $0.615\mu_B$.

Figure 18 shows the calculated magnetization vs Δ curves along the f-a line. The magnetization monotonically decreases and the first-order phase transition from the ferro- to the paramagnetic state occurs with increasing Δ for $N=9.1$. This behavior is explained by the shift of the main peak to the lower-energy region, leading to the decrease of DOS at the Fermi level (see Fig. 4). The magnetization for $N=9.0$ also decreases first with increasing Δ, but tends to become constant beyond $\Delta^{1/2}\approx 0.065$. It decreases and vanishes at $\Delta^{1/2}=0.077$ when we change $\Delta^{1/2}$ from 0.067 to 0.080 along the a-l line. This is again explained by the decrease of the noninteracting DOS $[\rho(0)]_s$ at the Fermi level due to structural disorder. The magnetization curves for $N=9.0$ seem to explain the experimental data $M=0.615\mu_B$ for the fcc Ni ($\Delta^{1/2}=0.0$), $M=0.45\mu_B$ for amorphous Ni ($\Delta^{1/2}\approx 0.063$) (Refs. 26 and 44), and $M=0.0\mu_B$ for liquid Ni ($\Delta^{1/2}=0.083$) (Refs. 29 and 42) as shown in Fig. 18.

Calculated inverse susceptibilities show the Curie-Weiss law at high temperatures. The effective Bohr magneton number rapidly increases beyond $\Delta^{1/2}\approx 0.06$ with the appearance of weak ferromagnetism.

The calculated Curie temperature for Ni is presented in Fig. 19 as a function of Δ. The Curie temperature monotonically decreases with increasing Δ for both $N=9.0$ and $N=9.1$. It decreases further along the a-l line and vanishes at $\Delta^{1/2}=0.08$. These behaviors demonstrate that more structural disorder yields lower Curie temperature in Ni and therefore explain qualitatively the change in experimental T_C from the fcc to amorphous and liquid structures in Ni. In particular, we predict from the experimental data presented in Fig. 1 that Δ(Ni-Y)$>\Delta$(Ni-La) around 90 at. % Ni.

IV. SUMMARY

We have developed a theory of metallic magnetism that interpolates between crystals and amorphous structures. The theory is based on the functional integral technique describing spin fluctuations at finite temperatures and the distribution function method describing the fluctuations of LM's due to structural disorder. The electronic structures in the intermediate region are specified by the fluctuation of interatomic distance Δ and the average coordination number z^* in the present theory.

We applied our theory to Fe, Co, and Ni and demonstrated that the magnetism changes drastically depending on the degree of structural disorder specified by a set of (z^*,Δ). In Fe, we have shown that the introduction of structural disorder decreases the magnetization along the b-a and b-c-a lines. The transition from the ferromagnetism to the SG occurs at $z^*=10.7$ and $\Delta^{1/2}=0.06$ ($z^*=10.6$ and $\Delta^{1/2}=0.04$) along the line b-a (b-c-a). The ferromagnetism is, how-

ever, enhanced when we increase Δ with constant z^* along the c-l line. The SG with $T_g = 110$ K in Fe-rich Fe-Zr, Fe-Y, and Fe-La alloys with more than 90 at. % Fe are explained by a structure $(z^*, \Delta) \approx (11.5, 0.067)$ along the b-a or b-c-a line, while the ferromagnetism of Fe-rich Fe-B alloys with more than 90 at. % Fe and the ''amorphous Fe'' with contamination of several wt. % H, C, and O can be explained by a structure $(z^*, \Delta) \approx (10.5, 0.07)$ along the c-l line. We also found the RSG at the boundary between F and SG states, which are realized by a change in detailed balance between F and AF couplings caused by a melt of LM's having AF couplings.

We have verified that the ferromagnetism in Co is monotonically enhanced with the introduction of structural disorder along both the f-a and b-a lines, so that there is no maximum in T_C in the intermediate regime. In Ni, the ferromagnetism is weakened with the introduction of structural disorder, but the results are rather sensitive to the d electron number N. The results with $N = 9.0$ along the f-a-l line explain the ferromagnetism in fcc Ni, the weak ferromagnetism in amorphous Ni, and the paramagnetism in a liquid structure. We have also explained the different Curie temperature obtained from amorphous Ni-Y and Ni-La alloys by means of the different Δ along the f-a line: $\Delta(\text{Ni-Y}) > \Delta(\text{Ni-La})$.

These conclusions show that the degree of structural disorder plays an important role in the basic magnetism of amorphous metals and alloys. Simultaneous measurements of structures and magnetic properties are therefore indispensable for the understanding of the amorphous metallic magnetism.

ACKNOWLEDGMENT

This work was partly supported by the Grant-in-Aid for Scientific Research from the Ministry of Education, Science, and Culture in Japan.

*Present address: Department of Physics and Astronomy, Ohio University, Athen, OH 45701.

[1] K. Fukamichi, T. Goto, H. Komatsu, and H. Wakabayashi, in *Proceedings of the Fourth International Conference on the Physics of Magnetic Materials, Poland, 1988*, edited by W. Gorkowski, H. K. Lachowicz, and H. Szymczak (World Scientific, Singapore, 1989), p. 354.

[2] P. Hansen, in *Handbook of Magnetic Materials*, edited by K. H. J. Bushow (North-Holland, Amsterdam, 1991), Vol. 6, p. 289.

[3] J. A. Fernandez-Baca and W. Y. Ching, *The Magnetism of Amorphous Metals and Alloys* (World Scientific, Singapore, 1995).

[4] H. Hiroyoshi and K. Fukamichi, Phys. Lett. **85A**, 242 (1981); J. Appl. Phys. **53**, 2226 (1982).

[5] N. Saito, H. Hiroyoshi, K. Fukamichi, and Y. Nakagawa, J. Phys. F **16**, 911 (1986).

[6] J. M. D. Coey, D. H. Ryan, and R. Buder, Phys. Rev. Lett. **26**, 385 (1987).

[7] D. H. Ryan, J. M. D. Coey, E. Batalla, Z. Altounian, and J. O. Ström-Olsen, Phys. Rev. B **35**, 8630 (1987); J. M. D. Coey, D. H. Ryan, and Yu Boliang, J. Appl. Phys. **55**, 1800 (1984); J. M. D. Coey and D. H. Ryan, IEEE Trans. Magn. **MAG-20**, 1278 (1984).

[8] H. Tange, Y. Tanaka, M. Goto, and K. Fukamichi, J. Magn. Magn. Mater. **81**, L243 (1989).

[9] J. A. Fernandez-Baca, J. J. Rhyne, G. E. Fish, M. Hennion, and B. Hennion, J. Appl. Phys. **67**, 5223 (1990).

[10] G. K. Nicolaides and K. V. Rao, J. Magn. Magn. Mater. **125**, 195 (1993).

[11] Y. Kakehashi, Phys. Rev. B **40**, 11 059 (1989).

[12] Y. Kakehashi, Phys. Rev. B **41**, 9207 (1990).

[13] Y. Kakehashi, Phys. Rev. B **43**, 10 820 (1991); **47**, 3185 (1993).

[14] M. Yu, Y. Kakehashi, and H. Tanaka, Phys. Rev. B **49**, 352 (1994).

[15] J. Hubbard, Phys. Rev. B **19**, 2626 (1979); **20**, 4584 (1979); **23**, 597 (1981).

[16] H. Hasegawa, J. Phys. Soc. Jpn. **46**, 1504 (1979); **49**, 178 (1980).

[17] Y. Kakehashi, Phys. Rev. B **34**, 3243 (1986).

[18] F. Matsubara, Prog. Theor. Phys. **52**, 1124 (1974); S. Katsura, S. Fujiki, and S. Inawashiro, J. Phys. C **12**, 2839 (1979).

[19] R. Hasegawa and R. Ray, J. Appl. Phys. **49**, 4174 (1978); S. Hatta and T. Egami, *ibid.* **50**, 1589 (1979); C. L. Chien and K. M. Unruh, Phys. Rev. B **24**, 1556 (1981); **25**, 5790 (1982); T. Stobiecki and F. Stobiecki, J. Magn. Magn. Mater. **35**, 217 (1983); G. Bayreuther, G. Enders, H. Hoffmann, V. Korndörfer, W. Oesterricher, K. Röll, and M. Takahashi, *ibid.* **31-34**, 1535 (1983); Z. Xianyu, Y. Ishikawa, S. Ishio, and M. Takahashi, J. Phys. F **15**, 1787 (1985).

[20] S. Krompiewski, U. Krey, and U. Krauss, J. Magn. Magn. Mater. **73**, 5 (1988); **69**, 117 (1987).

[21] A. M. Bratkovsky and A. V. Smirnov, Phys. Rev. B **48**, 9606 (1993).

[22] J. Hafner, M. Tegze, and Ch. Becker, Phys. Rev. B **49**, 285 (1994).

[23] S. Handschuh, J. Landes, U. Köbler, Ch. Sauer, G. Kisters, A. Fuss, and W. Zinn, J. Magn. Magn. Mater. **119**, 254 (1993).

[24] R. Bellissent, G. Galli, M. W. Grinstaff, P. Migliardo, and K. S. Suslick, Phys. Rev. B **48**, 15 797 (1993).

[25] M. Yu and Y. Kakehashi, Phys. Rev. B **49**, 15 723 (1994).

[26] A. Liénard and J. P. Rebouillat, J. Appl. Phys. **49**, 1680 (1978); A. Fujita, T. H. Chang, N. Kataoka, and K. Fukamichi, J. Phys. Soc. Jpn. **62**, 2579 (1993).

[27] R. Morel, L. Abadli, and R. W. Cochrane, J. Appl. Phys. **67**, 5790 (1990).

[28] H. Wakabayashi, K. Fukamichi, H. Komatsu, T. Goto, and K. Kuroda, in *Proceedings of the International Symposium on Physics of Magnetic Materials*, edited by W. Gorkowski, H. K. Lachowicz, and H. Szymczak (World Scientific, Singapore, 1987), p. 342.

[29] Y. Nakagawa, J. Phys. Soc. Jpn. **11**, 855 (1956); **12**, 700 (1957); I. Renz and S. Methfessel, J. Phys. (Paris), Colloq. **49**, C8-119 (1988).

[30] K. Fukamichi, T. Goto, and U. Mizutani, IEEE Trans. Magn. **MAG-23**, 3590 (1987).

[31] U. K. Poulsen, J. Kollár, and O. K. Andersen, J. Phys. F **6**, L241 (1976).

[32] O. K. Andersen, O. Jepsen, and D. Glötzel, in *Highlights of Condensed Matter Theory*, edited by F. Bassani, F. Fumi, and M. P. Tosi (North-Holland, New York, 1985).

[33] Y. Kakehashi, H. Tanaka, and M. Yu, Phys. Rev. B **47**, 7736 (1993).
[34] V. L. Moruzzi, J. F. Janak, and A. R. Williams, *Calculated Electronic Properties of Metals* (Pergamon, New York, 1978).
[35] T. Fujiwara, Nippon Butsuri Gakkaishi **40**, 209 (1985).
[36] M. Matsuura, H. Wakabayashi, T. Goto, H. Komatsu, and K. Fukamichi, J. Phys.: Condens. Matter **1**, 2077 (1989).
[37] R. Yamamoto and M. Doyama, J. Phys. F **9**, 617 (1979).
[38] H. Hasegawa, J. Phys. F **13**, 1915 (1983).
[39] Y. Kakehashi and M. Yu, Z. Phys. B **101**, 487 (1996).
[40] M. Yu and Y. Kakehashi, J. Phys.: Condens. Matter **8**, 5071 (1996).
[41] T. Ichikawa, Phys. Status Solidi A **19**, 707 (1973).
[42] Y. Waseda, *The Structure of Non-Crystalline Materials* (McGraw-Hill, New York, 1980).
[43] G. A. Prinz, Phys. Rev. Lett. **54**, 1051 (1985).
[44] A. Fujita (private communication).